



Patient-specific computational fluid dynamics of femoro-popliteal stent-graft thrombosis



Michele Conti^{a,*}, Anna Ferrarini^a, Alice Finotello^b, Giancarlo Salsano^c,
Ferdinando Auricchio^a, Domenico Palombo^d, Giovanni Spinella^d, Bianca Pane^d

^a Department of Civil Engineering and Architecture, University of Pavia, Via Ferrata 3, 27100 Pavia, Italy

^b Department of Surgical and Integrated Diagnostic Sciences, University of Genoa, Italy

^c Department of Radiology, IRCCS Ospedale Policlinico San Martino, Genoa, Italy

^d Vascular and Endovascular Surgery Unit, IRCCS Ospedale Policlinico San Martino, Genoa, Italy

ARTICLE INFO

Article history:

Received 28 January 2020

Revised 18 June 2020

Accepted 14 October 2020

Keywords:

Popliteal artery aneurysm

Peripheral stenting

Endovascular treatment

Femoro-popliteal segment

Medical image analysis

Limb flexion

Intra-stent thrombosis

Helicity

ABSTRACT

Intra-stent thrombosis is one of the major failure modes of popliteal aneurysm endovascular repair, especially when the diseased arterial segment is long and requires overlapping stent-grafts having different nominal diameters in order to accommodate the native arterial tapering.

However, the interplay between stent sizing, post-operative arterial tortuosity, luminal diameter, local hemodynamics, and thrombosis onset is not elucidated, yet.

In the present study, a popliteal aneurysm was treated with endovascular deployment of two overlapped stent-grafts, showing intra-stent thrombosis at one-year follow-up examination. Patient-specific computational fluid-dynamics analyses including straight- and bent-leg position were performed.

The computational fluid-dynamics analysis showed that the overlapping of the stent-grafts induces a severe discontinuity of lumen, dividing the stented artery in two regions: the proximal part, affected by thrombosis, is characterized by larger diameter, low tortuosity, low flow velocity, low helicity, and low wall shear stress; the distal part presents higher tortuosity and smaller lumen diameter promoting higher flow velocity, higher helicity, and higher wall shear stress. Moreover, leg bending induces an overall increase of arterial tortuosity and reduces flow velocity promoting further the luminal area exposed to low wall shear stress.

© 2020 The Authors. Published by Elsevier Ltd on behalf of IPPEM.

This is an open access article under the CC BY-NC-ND license

(<http://creativecommons.org/licenses/by-nc-nd/4.0/>)

1. Introduction

Popliteal artery aneurysms (PAAs) are the most frequent peripheral aneurysms [1]. PAA is treated when it reaches 2 cm in diameter, often by open surgery [2]; the endovascular treatment is one of the therapeutic options in elective cases, although it is still impaired by a lower rate of short-term patency and higher reintervention rate when compared with open surgical repair using prosthetic materials or autologous vein [3]. In particular, intra-stent thrombosis is still one of the long-term failures of femoro-popliteal endovascular treatments [4].

The mechanisms underpinning the onset and progression of femoro-popliteal intra-stent thrombosis are poorly investigated [5].

A recent meta-analysis of the literature confirmed that primary patency during follow-up is lower in patients undergoing endovascular treatment than in patients undergoing surgical treatment. However, if we consider secondary patency after one and three years of follow-up, it seems to be comparable between the two types of treatment [4]. Literature data reporting information regarding the follow-up intra-stent thrombosis are scarce because follow-up after endovascular treatment is often performed only through ultrasound examination or computed tomography angiography (CTA) performed shortly after treatment; all these factors can lead to underestimate the presence of an intra-stent thrombotic apposition [6,7].

Accordingly, the aim of the present study is to quantify the interplay among geometrical features and local hemodynamics inside femoro-popliteal endoprosthesis in a patient treated with endovascular stent-graft placement for PAA and complicated by intra-stent

* Corresponding author

E-mail address: michele.conti@unipv.it (M. Conti).

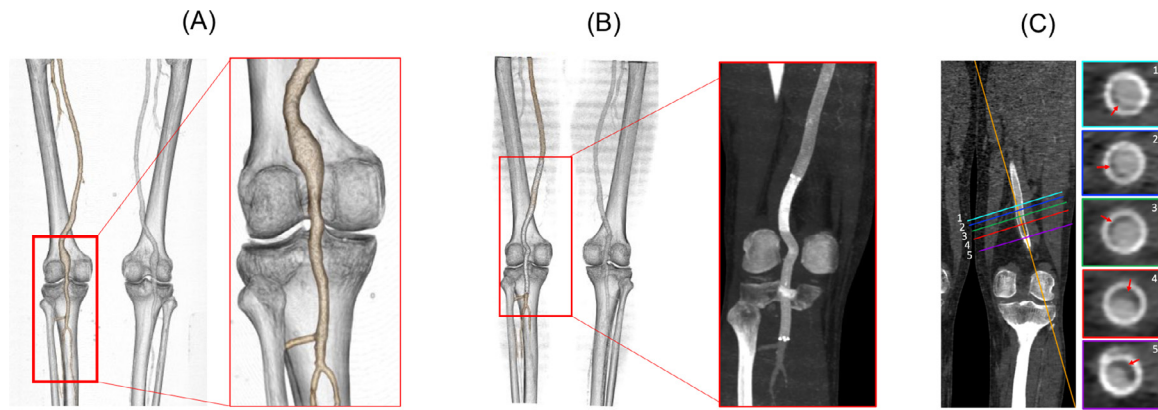


Fig. 1. A) pre-operative CTA reconstruction shows a popliteal aneurysm located just behind the knee. B) 1-year follow-up CTA with volume rendering and C) coronal view and five axial projections of intra-stent thrombosis highlighting its spiral evolution along the arterial axis.

thrombosis at one-year follow-up. In particular, we have performed patient-specific computational fluid-dynamics analysis based on 3D geometrical models derived from CTA images of the femoro-popliteal artery (FPA) segment covered with endovascular stent; moreover, both straight- and bent-leg position are considered in order to investigate the impact of leg bending on geometrical and hemodynamic features.

2. Materials and methods

2.1. Clinical case study

In 2017, a 77-year-old man underwent endovascular treatment for popliteal aneurysm. The patient was affected by an asymptomatic 30-mm popliteal aneurysm located just behind the knee (see Fig. 1A). In accordance with the preoperative planning, based on CTA, two self-expanding covered Viabahn stent-grafts (W.L. Gore & Associates, Flagstaff, AZ, USA) were positioned to cover the segment ranging from the distal superficial femoral artery to the popliteal artery up to the bifurcation with tibial artery: one 9×100 mm proximal stent-graft and one 7×100 mm distal stent-graft. According to the product's Instruction for Use, choice of different diameter stent-grafts was motivated by different diameter of the proximal (8 mm) and distal (6 mm) landing zones. The length of stent-grafts was chosen in order to cover the aneurysm and to obtain an adequate length of the proximal and distal landing zones.

The final angiographic check showed the correct positioning of the stents and the exclusion of the popliteal aneurysm. Unfortunately, the one-year follow-up CTA showed a partial thrombosis of the stent in the transition zone between the proximal and distal stent (see Fig. 1B and C).

2.2. Imaging acquisition protocol and image processing

According to the image acquisition protocol described in Spinella et al. [8] and approved by the Institutional Ethics Committee, two scans were performed during one-year follow-up CTA examination, in order to capture femoro-popliteal artery in both straight- and bent-leg position. In particular, during the first scan, the ipsilateral limb was placed in 90° position (bent-leg configuration) using a foam-coated support (see Fig. 2A), while the second acquisition was performed in straight-leg position. CTA scans were performed with a 64 multidetector-row CTA (General Electric Optima 660). The adopted scan parameters were: thickness, 0.625 mm; increment, 0.625 mm; collimation, 64×0.625 ; pitch, 0.915; rotation time, 0.7 s; field of view, 35 cm; matrix, 512×512 pixels.

Post-operative CTA images were anonymized and transferred to a workstation for image processing. Segmentation of the FPA segment (from the femoral artery bifurcation to the popliteal artery bifurcation), leg bones, intra-stent thrombosis, and implanted stent-grafts was performed using the open source tool Vascular Modeling ToolKit (VMTK, release 1.3). Briefly, a semiautomatic gradient-based level set segmentation process with colliding fronts initialization was adopted to extract the FPA lumen segment and the thrombotic region. A value of Hounsfield Units (HU) between 200 and 600 HU was adopted to initialize the segmentation of the lumen region, whereas values inferior to 200 HU identify the initialization of the thrombotic region. According to Kock et al. [9], sensitivity and specificity for detecting a $>50\%$ thrombosis were reported as 92% and 93%, respectively.

Leg bones were also extracted by semiautomatic gradient-based level set segmentation process with a threshold initialization method ($HU > 700$). An in-house Python code was developed to automatically extract the stent surface combining the CTA images and the information obtained by the segmented arterial lumen. Then, independently from the segmentation procedure, the zero level set surfaces are extracted using the Marching Cubes algorithm implemented in VMTK.

Rigid-registration of bent-leg structures on their corresponding straight-leg counterparts was performed by means of the Iterative Closest Point algorithm implemented in VMTK in order to allow a straightforward comparison between the 3D arterial models resulting from the two configurations (see Fig. 2B).

Vessel centerline was computed, resampled (resampling interval=0.5 mm), and smoothed by moving average filter [10] by means of VMTK scripts, in order to measure the luminal diameter and the arterial tortuosity in each zone [11]. Starting from the smoothed vessel centerline and the FPA lumen surface, equally spaced planes perpendicular to the centerline were automatically computed, and diameter measurements were taken on each transverse section. Tortuosity index was measured as a global parameter and was defined as $T = L/ED - 1$, where L is the centerline length, and ED is the shortest distance between the two centerline endpoints. Both parameters were automatically computed by means of VMTK scripts.

2.3. Patient-specific computational fluid dynamics (CFD)

Two 3D models were considered for the CFD simulations: 1) femoro-popliteal artery in straight-leg position; 2) femoro-popliteal artery in bent-leg position. Given our aim of understanding the reasons of the thrombosis onset and its localization along the lumen, the two models were derived removing the intra-stent

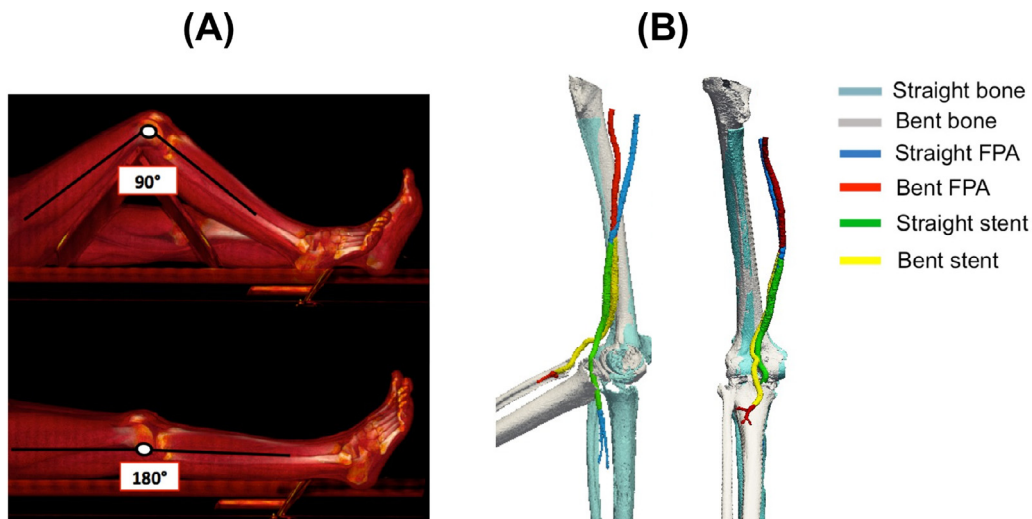


Fig. 2. A) Volume rendering of the CTA scan in bent-leg configuration – top picture – and in straight leg configuration – bottom picture. B) 3D models derived from image segmentation (left – lateral view, right – posterior view): bones, lumen, and stent-grafts are superimposed by rigid registration of the femur.

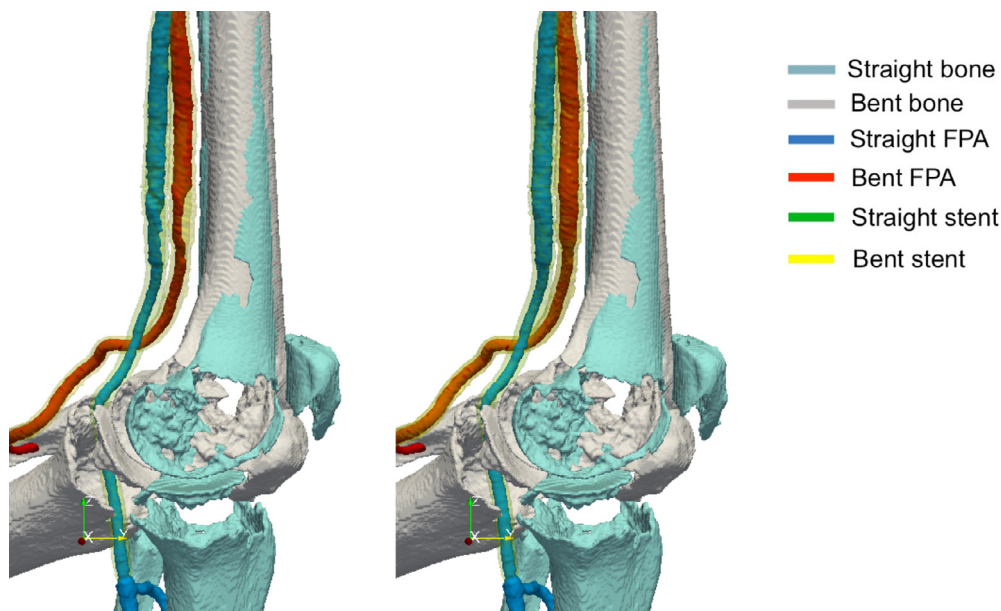


Fig. 3. Zoom view at the level of the knee of 3D models derived from image segmentation of superimposed bones, lumen, and stent-grafts in both leg configurations. On the left, the luminal model of the femoro-popliteal artery includes thrombosis, which is virtually removed to create the model resembling the pre-thrombosis lumen, used for CFD analyses (on the right).

thrombosis during the image segmentation, in order to define a surrogate pre-thrombotic condition (see Fig. 3).

Before generating the mesh, the geometries were smoothed and a flow-extension was added to the inlet of each model for ensuring that the numerical solution in the region of interest is not strongly affected by the selected inflow velocity profile. According to mesh convergence analysis, uniform meshes were generated with 651,635 total number of elements for the straight-leg model and with 569,817 total number of elements for the bent-leg model, in order to ensure an adequate accuracy of the numerical model [12,17]. Both preparing phase and generation of meshes were performed using the software VMTK [13]. Simulations were run in Intel Xeon W-2123 computing workstation (3.6 GHz, 32GB RAM) with the commercial CFD software package ANSYS Fluent (ANSYS Academic Research [Fluent], release 19.2). We performed transient simulations, in which viscosity was set to $0.004 \text{ kg m}^{-1} \text{ s}^{-1}$ and blood density to 1060 kg/m^3 . Moreover, in each simulation we pre-

scribed the no-slip condition on the wall of the artery, an outflow condition (Dirichlet boundary condition) enforcing the flow in the anterior tibial artery to be 25% of the inflow, and traction-free condition in the other outlets, located far away from the region of interest. The inflow velocity curve is derived from literature [14,15]: we impose a flat profile at the inlet section with time-dependent magnitude, implemented in Ansys as a user defined routine. Simulations were run for four cardiac cycles in order to damp transitory states; the last cycle was used to compute the results. Each cardiac cycle corresponds to 0.741 s, in which the systolic peak occurs at 0.196 s; the time-step was set to 0.001 s. We selected a laminar model (ANSYS Academic Research [Fluent], release 19.2) for all the simulations because the peak Reynolds number at the inlet is 284. Semi-Implicit Method for Pressure Linked Equations (SIMPLE) to solve the Navier-Stokes equations and a second order scheme for both pressure and momentum spatial-discretization were used.

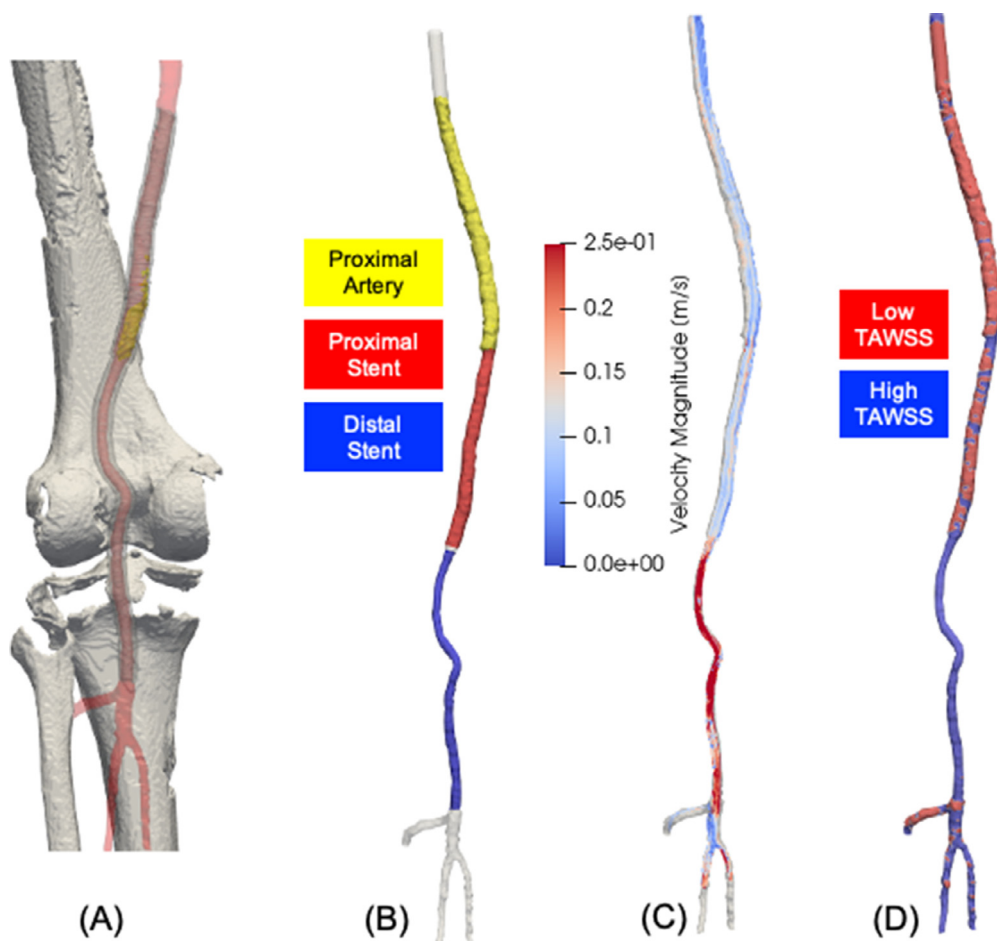


Fig. 4. (A) Posterior view of the femoro-popliteal artery in straight-leg configuration; (B) arterial lumen colored according to the three zones under investigation (proximal artery, proximal stent, and distal stent); (C) streamlines colored according to velocity magnitude at the systolic peak; (D) arterial lumen colored according to low (less or equal than 0.4 Pa) or high TAWSS (higher than 0.4 Pa).

2.4. Post-processing

We aim to set a proof of concept based on a case-study to be generalized by further investigation of a cohort of patients. Consequently, the definition of zones of interests that can be easily identifiable (e.g., proximal and distal stent) and the averaging of the results in these zones fits in such an aim. Moreover, the averaging of the results allows the damping of highly localized effects that often complicates the analysis of patient cohorts. Given such considerations, FPA axis was divided into three zones (see Fig. 4B): 1) proximal artery, i.e., lumen of the 10 cm artery above the proximal end of the proximal stent; 2) proximal stent, i.e., the lumen of the proximal stent, excluding the overlapping zone; 3) distal stent, i.e., the lumen of the distal stent including the overlapping zone (see Fig. 4A). In order to characterize the bulk flow features, flow velocity is averaged in space and time in each of the zones under investigation. Moreover, the vorticity vector field is computed and used to define local normalized helicity (LNH) [16], representing the normalized dot product between local velocity and vorticity vectors. Such an index allows the visualization of helical blood flow structures inside the artery. While LNH magnitude indicates the degree of local alignment of velocity and vorticity, its sign denotes the direction of rotation of helical structures, i.e., left- and right-handed blood structures inside the artery. Subsequently, the absolute value of the dot product of vorticity and velocity is averaged in space and time to compute the helicity intensity (h_2 index), an

indicator of the total amount of helical flow in the fluid domain, irrespective of direction [17]. Near wall flow features are described by the time-averaged wall shear stress (TAWSS); finally, the ratio of luminal surface exposed to low values, i.e., ranging between 0 and 0.4 Pa [18], with the whole luminal surface is computed, according with the experimental results of Zhan and coworkers [21], who showed that platelet adhesion increased with reduced wall shear stress.

3. Results

Fig. 4C–D shows the results of CFD analysis for the straight-leg configuration, reporting streamlines colored according to velocity magnitude at the systolic peak and the arterial lumen colored according to low (less or equal than 0.4 Pa) or high TAWSS (higher than 0.4 Pa).

Fig. 5 reports the bar-plots of luminal diameters, tortuosity, average flow velocity magnitude along the cardiac cycle, and the percentage of luminal surface exposed to low TAWSS for each zone (proximal artery, proximal stent, and distal stent) for both straight- and bent-leg configuration.

In the straight-leg configuration, the luminal diameters are 9.17 ± 0.74 mm, 7.85 ± 0.42 mm, and 4.90 ± 0.54 mm in the proximal artery, the proximal stent, and the distal stent zone, respectively. Such measurements do not vary significantly after leg bending; in fact, the luminal diameters in bent-leg configurations are

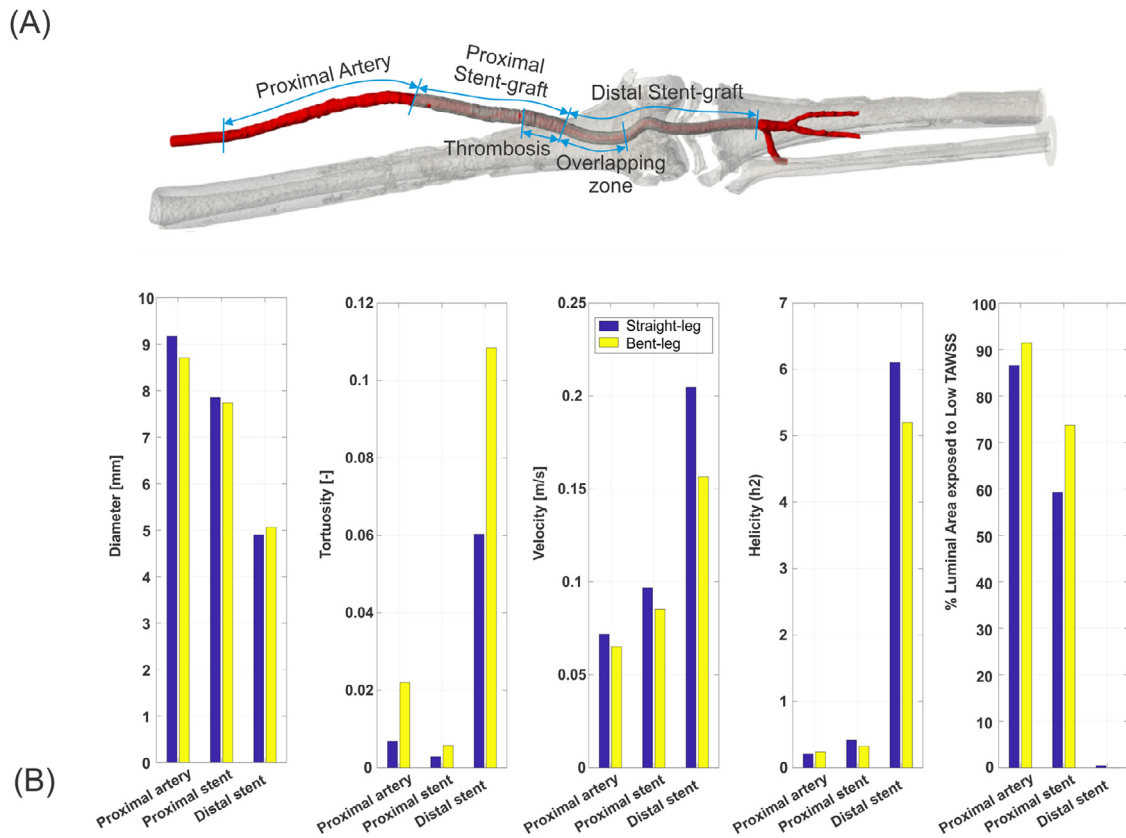


Fig. 5. Bar plot of luminal diameter, tortuosity, velocity magnitude averaged in space and time, helicity (h_2 -index), and percentage of luminal area exposed to low TAWSS. The data are reported for the three zones under investigation (proximal artery, proximal stent, and distal stent) in both leg configurations.

8.78±0.65 mm, 7.74±0.40 mm, and 5.06±0.27 mm in proximal artery, proximal stent, and distal stent zone, respectively. The size difference between two stent-grafts induces a difference of luminal diameters of almost 35%, resulting in a sudden jump of the luminal area localized at the beginning of the overlapping zone between the two stent-grafts. It is interesting to note that the thrombosis is located upstream of this jump in lumen diameters. Moreover, thrombosis has a spiral shape with counterclockwise evolution from distal to proximal direction.

In the straight-leg configuration, the tortuosity is 0.007, 0.003, and 0.06, respectively, in the area of the proximal artery, the proximal stent, and the distal stent; this result shows that the tortuosity is significantly higher in the distal stent area than in the proximal artery and in the proximal stent. Flexion of the leg increases the tortuosity of the proximal artery (0.02) and the distal stent (0.1), while the tortuosity of the proximal stent area keeps similar values to the straight leg configuration (0.06).

The average flow velocity magnitude along the cardiac cycle is lower in the proximal artery (0.072 m/s) and proximal stent (0.1 m/s) zone when compared with the magnitude of the velocity of the flow inside the distal stent-graft (0.2 m/s). The leg bending induces also an overall reduction of the velocity magnitude: 0.065 m/s, 0.09 m/s, and 0.16 m/s in proximal artery, proximal stent, and distal stent zone, respectively.

Analogously, the helicity (h_2 -index) is similar in the proximal artery (0.2 m/s²) and proximal stent zone (0.4 m/s²), being significantly lower than value computed in the distal stent zone (6.1 m/s²). Leg bending induces an overall decrease of the flow helicity intensity: 0.24, 0.32, and 5.2 m/s² in the proximal artery, the proximal stent, and the distal stent zone, respectively.

Finally, the proximal artery is highly exposed to low TAWSS in both leg configurations (straight-leg: 86.58%, bent-leg: 91.38%);

similarly, proximal stent zone shows a large area exposed to low TAWSS (straight-leg: 59.3%, bent-leg: 73.7%) while this is absent in distal stent zone (straight-leg: 0.5%, bent-leg: 0%).

Helical blood flow patterns developing into the endoprostheses are visualized in Fig. 6 using isosurfaces of LNH at the peak of the inflow velocity, where blue and red colors indicate respectively left-handed and right-handed helical flow rotation [19,20]. It is possible to observe a consistent flow pattern characterized by two counter-rotating flows, which keeps being stable along the whole cardiac cycle. Such a flow pattern is stronger in the distal stent as stated by the h_2 index. It is also interesting to see that the spiral shape of the thrombosis matches the path of the negative LNH region.

4. Discussions

Our results showed that the overlapping of the stent-grafts induces a severe discontinuity of lumen diameter, dividing the region treated with endovascular stent-graft in two zones: a) the proximal part, where thrombosis is located, is characterized by larger diameter, low tortuosity, low flow velocity, low helicity, and low TAWSS; b) the distal part, that presents higher tortuosity and smaller lumen diameter, promoting higher flow velocity, higher helicity, and higher TAWSS.

The indication that intra-stent thrombosis is located in the region where the intensity of helicity is low confirmed the crucial role of helical (or swirling flow) in the prevention of thrombosis. Such an indication has been previously reported by Zhan et al. [21] who, from the experimental tests, revealed that the swirling flow significantly reduces the adhesion of platelets to the inner surface of a glass tube when compared with the normal flow. Zhan and colleagues put forward the key concept that the blood

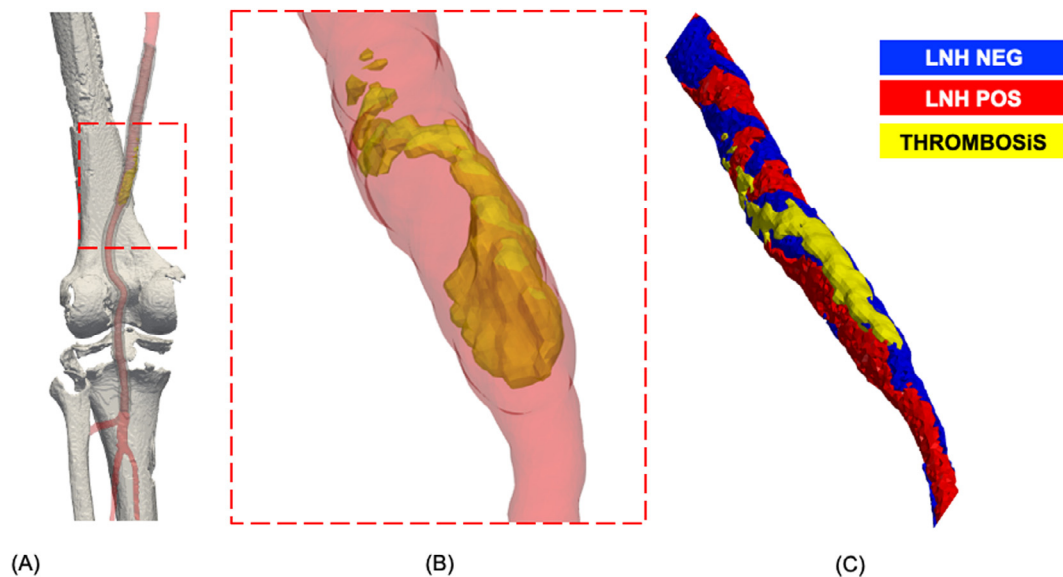


Fig. 6. (A) Posterior view of the femoro-popliteal artery in straight-leg configuration: the area where the thrombosis is localized is highlighted by a red box. (B) Zoom view of the lumen, in light red, with thrombosis (in yellow): it is possible to appreciate the helical shape of the thrombosis that evolves in an almost one turn from distal to proximal direction. (C) Blood flow helicity: in blue the flow with negative LNH and in red the flow with positive LNH. Superimposing the thrombosis (in yellow), it is possible to observe how it follows the helical shape of negative LNH region.

flow swirling in small diameter grafts promotes the blood velocity near the vessel wall and wall shear rate could be increased and, consequently, this hemodynamic condition can suppress the adhesion of platelets to the graft wall, impeding the occurrence of acute thrombus formation. Similar considerations have driven the seminal work of Caro et al. [22], who tested patented grafts with helical shapes [23] in a porcine model study, reporting consistently less thrombosis than conventional grafts. Caro and colleagues have even proposed a commercial self-expandable stent for femoro-popliteal disease, having a 3D helical centerline geometry set into a shape memory Nitinol material [24]. Our results suggest that the spiral shape of the thrombosis matches the path of the negative LNH region; it is hard to formulate a hypothesis to explain this result but, at the same time, it is intriguing to observe such a peculiar pattern. The consolidation and generalization of this result by the analysis of cohort of patients will surely provide more information to explain this observation, whether confirmed.

At the best of our knowledge, the present study is the first reporting patient-specific CFD analysis of both straight- and bent-leg femoro popliteal models derived from CTA. Indeed, Gökgöl and colleagues in a very recent study have proposed a similar approach considering 20 patients but the models were reconstructed from 2D angiographic images [25]. Despite the approach proposed by Gökgöl and colleagues has the benefit of being easily integrated into the clinical workflow, it is limited by the precision of the imaging system, being not able to capture localized crucial effects, such as the jump of luminal diameter in the overlapping stent-graft region. Very recently, investigating the impact of leg movement on FPA hemodynamics, Colombo et al. have proved the importance of accounting leg bending using idealized geometrical model of the vessel, calling for patient-specific FPA models reconstructed from clinical images [26].

Nevertheless, our study suggests that the leg flexion reduces the overall flow velocity, helicity, and TAWSS confirming the results reported by analysis of Gökgöl et al. [25], who showed that leg bending significantly modifies certain flow behaviors in stented arteries.

Finally, we found that the lumen area exposed to low shear stress increases after leg bending; this result matches the find-

ings of Schlager et al. [27], who performed velocity measurements in the femoro-popliteal arteries of 46 healthy subjects in supine and sitting positions, showing that the mean WSS significantly decreased when the patients were sitting; this indication is reported by Gökgöl et al., as well [25].

Our results confirm that stent sizing is crucial for popliteal stenting outcome. During the planning of endovascular treatment, an adequate proximal landing zone is fundamental for the success of the treatment [28,29]. When we take into consideration the femoro-popliteal axis in the planning of endovascular treatment, we should take into consideration the difference of diameters between the distal and proximal landing zone. In fact, in patients not affected by aneurysmal pathology of the popliteal femoral axis, the average diameter of the distal popliteal artery and the superficial femoral artery is approximately 4.4 mm and 7.3 mm, respectively. In patients with popliteal aneurysm, on the other hand, the average diameter of the distal popliteal artery is 6.4 mm and the superficial femoral artery of 8.4 mm [30]. Consequently, in the present case study, the diameter of the distal landing zone was 6 mm while the diameter of the proximal landing zone was 8 mm; therefore, using the recommended oversizing, a 7 mm diameter stent was used distally, and a 9 mm stent of diameter was used proximally. It is worth nothing that the choice of stent diameter is also done taking into consideration the need to avoid infolding of the stent graft that can then lead to stent occlusion [31,32]; in fact, an oversizing of the stent in more than 15% should be avoided [33]. Currently, the covered stents available on the market have a constant diameter and therefore it is necessary to use at least two stents when treating arteries with different proximal and distal diameters; this condition implies that along the stented region there could be a large variation of luminal caliber, as in the case under investigation.

5. Limitations

The present proof concept study is aiming at linking post-stenting geometry, hemodynamics, and thrombosis in endovascular repair of popliteal aneurysms. Based on the analysis of one case, our results cannot be generalized; consequently, further analyses addressing a large database of patients with similar characteristics

should be performed in order to withdraw statistically significant and clinically relevant conclusions.

The inflow data are taken from the literature [15]; patient-specific flow information will be included in future studies by elaborating echo doppler measurements as proposed by Colombo et al. [17].

We have created a surrogate geometrical model of the lumen prior to thrombosis by virtually removing the thrombus during the segmentation process. Such a limitation could be overcome by the analysis of CT scans performed at different time instants, from early post-operative to annual follow-up exams; unfortunately, the current standard clinical follow-up protocol for popliteal stenting foresees the use of echo-color doppler at 1, 6, 12 months follow-up, and yearly thereafter that does not allow to extract the vessel thrombosis. Although some centers are beginning to perform a CTA once during short-time follow-up, in general in the clinical practice a second level examination is prescribed only when intrastent stenosis or thrombotic apposition within the stent is found [7,34].

Thrombosis is a complex phenomenon that cannot be analyzed only from a fluid dynamics point of view as we have done in the present study. Artificial surfaces, such as the inner layer of stent-graft, promote clotting through a complex series of interconnected processes, from protein adsorption to adhesion of platelets, through thrombin generation and complement activation [35]. Further developments of the present study should consider the role of hemodynamic stress in the platelet activation [36], recently proved to be predictive of aortic thrombus formation following thoracic endovascular aortic repair [37]. Finally, stent struts are not taken into consideration in the present study; however, the stent struts have an effect on wall shear stress [38], further developments will target this aspect.

6. Conclusions

Although limited to single case, the results of the present study show that the overlapping zone of the stent-grafts induces a severe discontinuity of lumen, dividing the landing site in two segments: the proximal part, affected by thrombosis, is characterized by larger diameter, low tortuosity, low flow velocity, low helicity, and low TAWSS; the distal part presents higher tortuosity and smaller lumen diameter promoting higher flow velocity, higher helicity, and higher TAWSS. Moreover, leg bending induces an overall increase of arterial tortuosity and reduces the flow velocity promoting furtherly the luminal area exposed to low wall shear stress. Intra-stent thrombosis has a helical shape suggesting that there is an implication of flow helicity in the thrombosis onset and progression to be elucidated by further developments of the present study.

Declaration of Competing Interest

None declared.

Acknowledgments

Ministry of Health through the Ricerca Finalizzata Project no. RF-2018-12368376 entitled “Impact of peripheral endovascular repair on femoral-popliteal artery kinematic: from clinical experience to in vivo biomechanical modeling (PERFEKT study)”.

Funding

None.

Ethical approval

The study was approved by the Liguria Regional Ethics Committee (comitato etico regionale liguria) on 15/07/2019 (Ref. gr-2018-12368376; internal reference number 197/2019).

References

- [1] Szilagyi DE, Schwartz RL, Reddy DJ. Popliteal arterial aneurysms. Their natural history and management. *Arch Surg* 1981;116(5):724–8.
- [2] Galland RB. History of the management of popliteal artery aneurysms. *Eur J Vasc Endovasc Surg* 2008;35:466–72.
- [3] Lovegrove RE, Javid M, Magee TR, Galland RB. Endovascular and open approaches to non-thrombosed popliteal aneurysm repair: a meta-analysis. *Eur J Vasc Endovasc Surg* 2008;36(1):96–100. doi:10.1016/j.ejvs.2008.02.002.
- [4] Leake AE, Segal MA, Chaer RA, Eslami MH, Al-Khoury G, Makaroun MS, et al. Meta-analysis of open and endovascular repair of popliteal artery aneurysms. *J Vasc Surg* 2017;65(1):246–56.
- [5] Byrne RA, Joner M, Kastrati A. Stent thrombosis and restenosis: what have we learned and where are we going? The Andreas Gruentzig Lecture ESC 2014. *Eur Heart J* 2015;36:3320–31. doi:10.1093/eurheartj/ehv511.
- [6] Tielliu IF, Zeebregts CJ, Vourliotakis G, Bekkema F, van den Dungen JJ, Prins TR, et al. Stent fractures in the Hemobahn/Viabahn stent graft after endovascular popliteal aneurysm repair. *J Vasc Surg* 2010;51(6):1413–18.
- [7] Piazza M, Menegolo M, Ferrari A, Bonvini S, Ricotta JJ, Frigatti P, et al. Long-term outcomes and sac volume shrinkage after endovascular popliteal artery aneurysm repair. *Eur J Vasc Endovasc Surg* 2014;48(2):161–8.
- [8] Spinella G, Finotello A, Pane B, Salsano G, Mambrini S, Kamenskiy A, et al. In vivo morphological changes of the femoropopliteal arteries due to knee flexion after endovascular treatment of popliteal aneurysm. *J Endovasc Therapy* 2019. doi:10.1177/1526602819855441.
- [9] Kock MC, Dijkshoorn ML, Pattinama PM, Myriam Hunink MG. Multi-detector row computed tomography angiography of peripheral arterial disease. *Eur Radiol* 2007;17:3208–22.
- [10] Piccinelli M, Veneziani A, Steinman DA, Remuzzi A, Antiga L. A framework for geometric analysis of vascular structures: application to cerebral aneurysms. *IEEE Trans Biomed Eng* 2009;28:1141–55.
- [11] Thomas JB, Antiga L, Che SL, Milner JS, Hangan Steinman DA, Spence JD, et al. Variation in the carotid bifurcation geometry of young versus older adults: implications for geometric risk of atherosclerosis. *Stroke* 2005;36(11):2450–6.
- [12] Xu P, Liu X, Song Q, Chen G, Wang D, Zhang H, et al. Patient-specific structural effects on hemodynamics in the ischemic lower limb artery. *Sci Rep* 2016;6:39225.
- [13] Antiga L, Piccinelli M, Botti E, Ene-Iordache B, Remuzzi A, Steinman DA. An image-based modeling framework for patient-specific computational hemodynamics. *Med Biol Eng Comput* 2008;46:1097–112.
- [14] Desyatova A, MacTaggart J, Romarowski R, Poulson W, Conti M, Kamenskiy A. Effect of aging on mechanical stresses, deformations, and hemodynamics in human femoro-popliteal artery due to limb flexion. *Biomech Model Mechanobiol* 2018;17(1):181–9.
- [15] Patel DJ, Greenfield JC, Austen WG, Morrow AG, Fry DL. Pressure-flow relationships in the ascending aorta and femoral artery of man. *J Appl Physiol* 1965;20:459–63.
- [16] Morbiducci U, Ponzini R, Grigioni M, Redaelli A. Helical flow as fluid dynamic signature for atherogenesis risk in aortocoronary bypass. A numeric study. *J Biomech* 2007;40:519–34.
- [17] Colombo M, Bologna M, Garbey M, Berceci S, He Y, Matas JFR, et al. Computing patient-specific hemodynamics in stented femoral artery models obtained from computed tomography using a validated 3D reconstruction method. *Med Eng Phys* 2020;75:23–35.
- [18] Malek AM, Alper SL, Izumo S. Hemodynamic shear stress and its role in atherosclerosis. *JAMA* 1999;282(21):2035–42.
- [19] Gallo D, Steinman DA, Bijari PB, Morbiducci U. Helical flow in carotid bifurcation as surrogate marker of exposure to disturbed shear. *J Biomech* 2012;45:2398–404.
- [20] Morbiducci U, Ponzini R, Gallo D, Bignardi C, Rizzo G. Inflow boundary conditions for image-based computational hemodynamics: impact of idealized versus measured velocity profiles in the human aorta. *J Biomech* 2013;46:102–9.
- [21] Zhan F, Fan Y, Deng X. Swirling flow created in a glass tube suppressed platelet adhesion to the surface of the tube: its implication in the design of small-caliber arterial grafts. *Thromb. Res.* 2010;125(5):413–18.
- [22] Caro C, Cheshire N, Watkins N. Preliminary comparative study of small amplitude helical and conventional ePTFE arteriovenous shunts in pigs. *J R Soc Interface* 2005;2:261–6.
- [23] Caro C, Watkins N, Sherwin S. Helical graft. Patent US 2007/0021707 A1 2007.
- [24] Zeller T, Gaines PA, Ansel GM, Caro CG. Helical centerline stent improves patency: two-year results from the randomized mimics trial. *Circul: Cardiovasc Interv* 2016;9(6):e002930.
- [25] Gököl C, Diehm N, Räber L, Büchler P. Prediction of restenosis based on hemodynamical markers in revascularized femoro-popliteal arteries during leg flexion. *Biomech Model Mechanobiol* 2019;18:1883–93.

- [26] Colombo M, Luraghi G, Cestariolo L, Ravasi M, Airoidi A, Chiastra C, Pennati G. Impact of lower limb movement on the hemodynamics of femoropopliteal arteries: a computational study. *Med Eng Phys* 2020;81:105–17.
- [27] Schlager O, Giurgea A, Margeta C, Seidinger D, Steiner-Boecker S, van der Loo B. Wall shear stress in the superficial femoral artery of healthy adults and its response to postural changes and exercise. *Eur J Vasc Endovasc Surg* 2011;41:821–7.
- [28] Siauw R, Koh EH, Walker SR. Endovascular repair of popliteal artery aneurysms: techniques, current evidence and recent experience. *ANZ J Surg* 2006;76:505e11.
- [29] Garg K, Rockman CB, Kim BJ, Jacobowitz GR, Maldonado TS, Adelman MA, et al. Outcome of endovascular repair of popliteal artery aneurysm using the Viabahn endoprosthesis. *J Vasc Surg* 2012;55:1647e53.
- [30] Wolf YG, Kobzantsev Z, Zelmanovich L. Size of normal and aneurysmal popliteal arteries: a duplex ultrasound study. *J. Vasc. Surg.* 2006;43(3):488–92.
- [31] Cook S, Windecker S. Early stent thrombosis: past, present, and future. *Circulation* 2009;119:657–9 35.
- [32] van Sambeek MR, Gussenhoven EJ, van der Lugt A, Honkoop J, du Bois NA, van Urk H. Endovascular stentgrafts for aneurysms of the femoral and popliteal arteries. *Ann Vasc Surg* 1999;13:247e53.
- [33] Trinidad-Hernandez M, Ricotta JJ II, Gloviczki P, Kalra M, Oderich GS, Duncan AA, et al. Results of elective and emergency endovascular repairs of popliteal artery aneurysms. *J. Vasc. Surg.* 2013;57(5):1299–305.
- [34] Pineda DM, Troutman DA, Dougherty MJ, Calligaro KD. Surveillance duplex ultrasonography of stent grafts for popliteal aneurysms. *Vasc Endovasc Surg* 2016;50(4):231–4.
- [35] Jaffer IH, Fredenburgh JC, Hirsh J, Weitz JL. Medical device-induced thrombosis: what causes it and how can we prevent it? *J Thromb Haemost* 2015;13:S72–81.
- [36] Shadden SC, Hendabadi S. Potential fluid mechanic pathways of platelet activation. *Biomech Model Mechanobiol* 2013;12(3):467–74 .
- [37] Nauta FJ, Lau KD, Arthurs CJ, Eagle KA, Williams DM, Trimarchi S, et al. Computational fluid dynamics and aortic thrombus formation following thoracic endovascular aortic repair. *Ann. Thorac. Surg.* 2017;103(6):1914–21.
- [38] Al-Hakim R, Lee EW, Kee ST, Seals K, Varghese B, Chien A, Quirk M, McWilliams J. Hemodynamic analysis of edge stenosis in peripheral artery stent grafts. *Diagn Interv Imaging* 2017;98(10):729–35.